ChemComm

COMMUNICATION

View Article Online
View Journal | View Issue

Cite this: *Chem. Commun.*, 2025, **61**, 961

Received 26th November 2024,
Accepted 10th December 2024

DOI: 10.1039/d4cc06281g

rsc.li/chemcomm

CoP electrocatalysts embedded in nitrogen-doped carbon as a host toward fast iodine conversions†

Lingfeng Zhu,[abc] Xinwei Guan,[b] Zhenfang Zhang,[b] Yang Fu,[b] Zhilong Yuan,[a] Congcong Zhang,[a] Ye Wang,[a] Hua Fan,[d] Haimei Xu,[b] Xiaoning Li,[b] Hui Li,[b] Baohua Jia,[b] Hai Yu,[c] Yifei Sun *[aef] and Tianyi Ma *[b]

Herein, well-dispersed cobalt phosphide (CoP) electrocatalysts embedded in nitrogen-doped carbon (CoP@NC) were developed as an iodine host for zinc iodine batteries. Benefiting from the high electrical conductivity of the carbon matrix and the strong interaction as well as the efficient electrocatalytic activity of CoP with iodine species, the host achieved rapid iodine conversion while effectively suppressing the formation of polyiodides and zinc dendrites.

In recent years, lithium-ion batteries have faced challenges in meeting the growing demand for energy storage due to their high cost and safety risks, which has triggered the rapid development of alternative rechargeable batteries with high energy density, enhanced safety, and environmental sustainability. Among these, aqueous zinc–iodine batteries (AZIBs) have garnered significant attention from researchers due to their low cost, high safety and high capacity.[1,2] However, the inherent poor conductivity of iodine ($\sim 10^{-6}$ S cm^{-1}) severely hinders the iodine redox kinetics. Moreover, the shuttle effect, where iodine forms polyiodide intermediates (I_3^- and I_5^-) during cycling, results in irreversible loss of active mass, severe self-discharge, and corrosion of the zinc anode.[2]

To address these challenges, researchers have explored porous carbon-based materials as iodine hosts, such as carbon fibers,[3] nanosheets,[4] and porous carbon[5] to inhibit the dissolution and shuttling of polyiodides. However, the weak van der Waals forces of non-polar carbon materials are insufficient to provide stable polyiodide inhibition during the cycling process. Therefore, introducing electrocatalysts to catalyze iodine conversion reactions and enhance the stable chemical adsorption of iodine species presents a promising strategy for improving the iodine conversion kinetics.

Metal phosphides have the characteristics of low cost, high conductivity and the ability to accelerate redox reactions, making them widely studied in electrocatalysis and lithium–sulfur batteries.[6,7] For example, Sun *et al.*[6] synthesized CoP nanoparticles/carbon nanocages, achieving a high capacity of 622 mA h g^{-1} at 5C in a Li–S battery by enhanced S redox kinetics. Similarly, Ji *et al.*[7] developed CoP nanoframes that exhibited impressive bifunctional catalytic activities for both the HER and OER. Recently, a Ni_2P@C host has been developed and showed a promoting effect on the iodine's redox in AZIBs.[8] These applications have greatly inspired us to explore the potential of metal phosphide hosts in catalyzing iodine's redox kinetics. However, highly surface-active CoP particles are prone to agglomerate, significantly reducing their catalytic sites. Here, integrating carbon materials with CoP nanoparticles offers a viable strategy to balance catalytic sites and improve iodine conductivity. First, the carbon matrix can effectively prevent the aggregation of CoP nanoparticles.[9] Second, nitrogen-doped carbon materials can greatly enhance the conductivity of the composite, accelerating the redox kinetics.[2] Notably, CoP has not been reported in AZIBs, and the fundamental understanding of its intrinsic mechanism for accelerating the redox of iodine remains to be fully elucidated.

Herein, well-dispersed CoP electrocatalysts embedded in a nitrogen-doped carbon matrix (CoP@NC) were customized *via* a simple pyrolysis and vapor-phase phosphating method. The CoP@NC host not only demonstrates strong chemical affinity to inhibit the polyiodide's penetration, but also offers abundant catalysis sites to promote iodine redox kinetics (I_2 to I^-). At the same time, the n-doped carbon matrix can further enhance the conductivity of the composite and provide sufficient interfaces to load iodine. Consequently, the CoP@NC/I_2 exhibits a superior high-rate capacity of 191.1 mA h g^{-1} at 0.1 A g^{-1} and

[a] *School of Energy and Power Engineering, Beihang University, Beijing, 100191, China. E-mail: sunif@buaa.edu.cn*
[b] *Centre for Atomaterials and Nanomanufacturing (CAN), School of Science, RMIT University, Melbourne, VIC, 3000, Australia. E-mail: tianyi.ma@rmit.edu.au*
[c] *CSIRO Energy, 10 Murray Dwyer Circuit, Mayfield West, NSW 2304, Australia*
[d] *Aqualux AU Pty Ltd, 12 Kanangra Cres, Clontarf, NSW 2093, Australia*
[e] *Research Center for Advanced Energy and Carbon Neutrality, Beihang University, Beijing 100191, China*
[f] *School of Environmental Science and Engineering, Hainan University, Haikou, 570228, China*

† Electronic supplementary information (ESI) available. See DOI: https://doi.org/10.1039/d4cc06281g

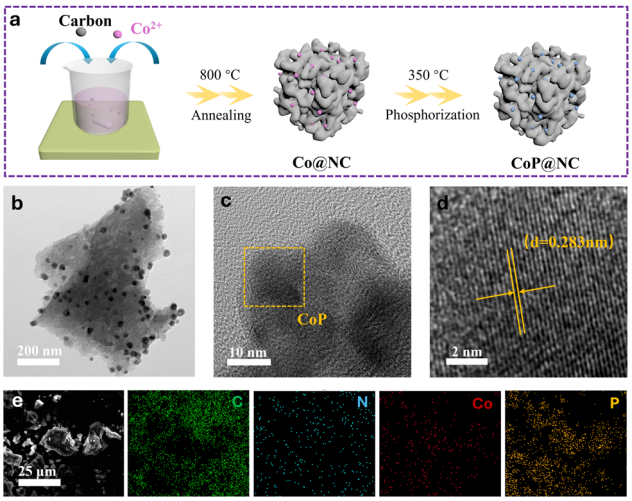

Fig. 1 (a) Schematic illustration of the synthesis process for the CoP@NC host, (b) TEM images, (c) and (d) high-resolution TEM images, and (e) SEM image with element mappings of CoP@NC.

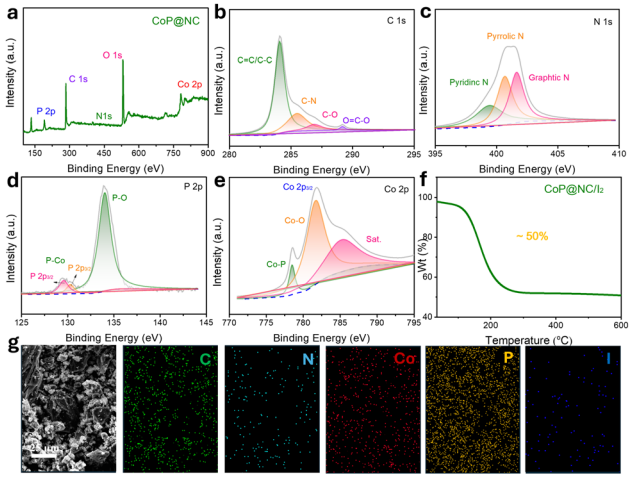

Fig. 2 (a) XPS survey spectrum of CoP@NC. (b)–(e) High-resolution XPS spectra of C 1s, N 1s, P 2p and Co 2p of CoP@NC. (f) TGA curves of CoP@NC/I_2. (g) SEM image with EDS images of CoP@NC/I_2.

superior cycling stability of 101.4 mA h g^{-1} with around 100% coulomb efficiency (CE) after 1000 cycles at 1.0 A g^{-1}. These results highlight the outstanding performance of CoP@NC as an iodine host, establishing it as a competitive candidate among metal phosphide-based materials for AZIBs. Our work provides new insights into developing high-performance metal phosphide-based host materials for AZIBs.

The CoP@NC was prepared using a two-step strategy involving pyrolysis and phosphidation (Fig. 1a). The structure of CoP@NC was identified by X-ray diffraction (XRD) first. Fig. S1 (ESI†) displays obvious diffraction peaks at ~31.5, 35.2, 36.3, 46.1, 48.0, 52.2, 56.0 and 56.7, which are indexed to the CoP phase (PDF# 65-2593), without an impurity phase of cobalt oxide.[10] Transmission electron microscopy (TEM) in Fig. 1b showed that the CoP nanoparticles are evenly dispersed on the n-doped carbon with an average size of ~22 nm (Fig. S2, ESI†). The high-resolution TEM (HRTEM) image further demonstrated the crystalline nature of the CoP (Fig. 1c), and the regular crystalline fringes with a *d*-spacing value of 0.283 nm can be observed in Fig. 1d, correspond to the (011) lattice plane of metallic CoP.[11] This result is consistent with the XRD's conclusion. The scanning electron microscope (SEM) and elemental distribution mapping (EDS) images further confirmed the uniform distribution of C, N, Co, and P elements throughout the CoP@NC (Fig. 1e), validating the successful integration of CoP within the nitrogen-doped carbon matrix.

The surface chemical states of the CoP@NC were studied using X-ray photoelectron spectroscopy (XPS). As shown in Fig. 2a, the survey XPS spectra confirmed the presence of C, N, Co, and P elements in CoP@NC. Specifically, the high-resolution XPS spectrum of C 1s in Fig. 2b revealed four types of carbon species, namely C=C/C–C in 284.0 eV, C–N in 285.4 eV, C–O in 286.8 eV and O=C–O in 289.1 eV, respectively.[12,13] For the N 1s spectrum, three characteristic N types – pyridine N, pyrrolic N and graphitic N can be observed at binding energies of 399.4, 400.6 and 401.6 eV, respectively (Fig. 2c). These nitrogen dopants can increase the conductivity of the composites and facilitate the redox reaction kinetics.[14,15] Moreover, the P 2p spectra in Fig. 2d exhibited peaks at 134.0, 130.3 and 129.5 eV. The former peak belongs to the P–O bonds, while the latter two weak peaks are assigned to the P–Co bond (Co $2p_{3/2}$ and Co $2p_{1/2}$).[10] The Co 2p spectrum (Fig. 2e) further corroborated the presence of CoP, with peaks assigned to Co–P (778.5 eV), a satellite peak (785.1 eV) and Co–O (781.6 eV).[16,17] This Co–O is caused by the surface oxidation of the CoP@NC.[7] Notably, the Co $2p_{3/2}$ in CoP@NC shifted positively (778.5 eV), compared with the Co (778.1 eV) in pure CoP, indicating a strong interfacial coupling between CoP and the N-doped carbon substrate.[18,19] These results collectively confirmed the successful incorporation of CoP electrocatalyst into the n-doped carbon matrix, with well-defined bonding configurations supporting its catalytic properties.

Subsequently, the CoP@NC's ability to serve as an iodine host was further evaluated, and the CoP@NC/I_2 cathode was obtained through a melt-diffusion strategy (Fig. S3, ESI†). The mass content of I_2 in the CoP@NC/I_2 was determined to be ~50 wt%, as calculated from the thermogravimetric analysis (TGA) curve (Fig. 2f). The stable iodine-carrying properties can be attributed to the synergistic effect of the physical confinement provided by the carbon matrix and the strong chemical adsorption of iodine by the CoP, which laid the foundation for the subsequent rapid and efficient iodine redox. Furthermore, SEM and EDS images of CoP@NC/I_2 confirmed the uniform distribution of I_2 in CoP@NC (Fig. 2g).

Leveraging the great potential of CoP@NC as a host material, the electrochemical performance of the CoP@NC/I_2 cathode was systematically studied in AZIBs. As shown in Fig. 3a, the CoP@NC/I_2 cathode delivered high reversible rate capacities of 191.1, 161.5, 138.9, 120.8, and 107.1 mA h g^{-1} at 0.1, 0.2, 0.5, 1.0, and 2.0 A g^{-1}, respectively, which are higher than that of the NC/I_2 cathode across all tested conditions. When the current density is recovered to 0.2 A g^{-1}, the CoP@NC/I_2

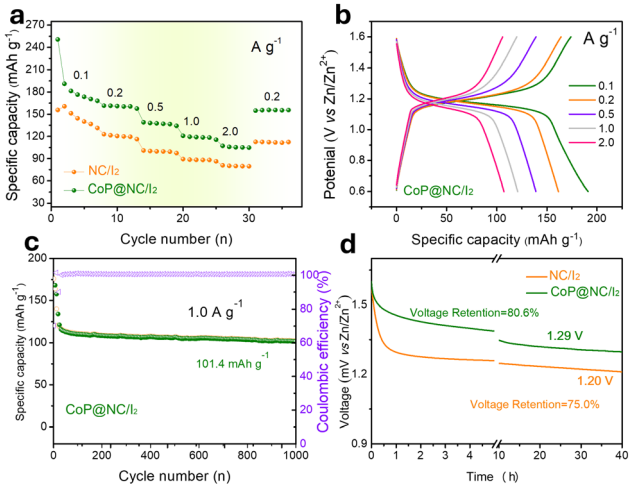

Fig. 3 (a) Rate capacity of CoP@NC/I_2 and NC/I_2. (b) Discharge/charge curves and (c) cycling performance of CoP@NC/I_2. (d) Self-discharge performance of CoP@NC/I_2 and NC/I_2.

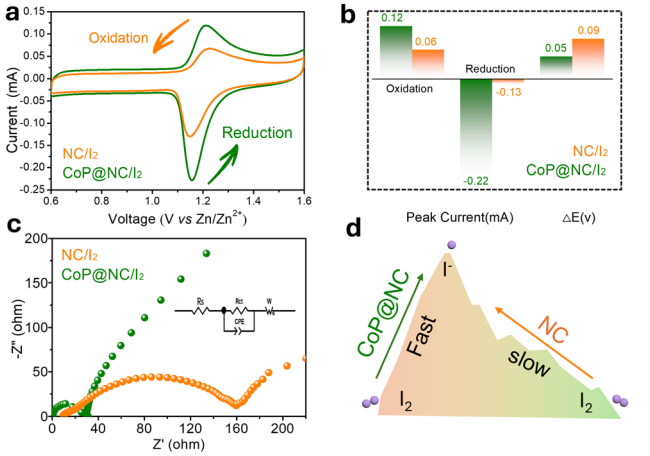

Fig. 4 (a) CV profiles, (b) the peak current and polarization voltage, and (c) EIS curves of CoP@NC/I_2 and NC/I_2. (d) Mechanism diagram illustrating the I_2 redox reaction.

cathode achieved a high specific capacity of 155.6 mA h g^{-1}, demonstrating its remarkable reversibility. In contrast, the NC/I_2 cathode only showed a poor performance of 113.4 mA h g^{-1} at 0.2 A g^{-1}. Besides, as the current density increases, the discharge/charge (GCD) curves of the CoP@NC/I_2 electrode maintained distinct plateaus, while the NC/I_2 electrode showed a rapid tightening trend, especially at high current density (Fig. 3b and Fig. S4, ESI†). These results indicated that the CoP@NC host can greatly improve iodine utilization. Notably, the rate performance of CoP@NC/I_2 was highly competitive compared to other reported Zn/I_2 battery hosts (Fig. S5, ESI†), underscoring its potential for advanced AZIBs.

The long-term cycling performance of both electrodes was evaluated in Fig. 3c. Specifically, the CoP@NC/I_2 cathode maintained a high capacity of 101.4 mA h g^{-1} with ~100% CE after 1000 cycles at 1.0 A g^{-1}, indicating the exceptional efficiency of its electrochemical redox reactions. Importantly, the CoP@NC/I_2 electrode also maintained a stable high voltage of 1.29 V over 40 h, while the NC/I_2 electrode just kept 1.20 V, indicating the excellent self-discharge performance of CoP@NC/I_2. This excellent performance may be due to the rapid adsorption-catalytic ability of the CoP@NC to iodine species, which greatly reduces the formation of polyiodide and improves the utilization efficiency of iodine.

To elucidate the excellent electrochemical performance of the CoP@NC/I_2 cathode, cyclic voltammetry (CV) and electrochemical impedance spectroscopy (EIS) tests were conducted to investigate the iodine conversion kinetics. As shown in Fig. 4a, the CV curves of both electrodes showed a pair of redox peaks at ~1.15/1.20 V at 0.2 mV s^{-1}, corresponding to the conversion from I_2 to I^-.[5] Notably, the CoP@NC/I_2 electrode exhibited a higher current (0.12/−0.22 mA) and a lower voltage polarization (0.05 V) compared to the NC/I_2 electrode, indicating significantly enhanced redox kinetics for the CoP@NC/I_2 electrode (Fig. 4b). Besides, Tafel plots derived from the CV data further support this finding.[16,20] As illustrated in Fig. S6 (ESI†), the CoP@NC/I_2 electrode exhibited a smaller Tafel slope for both oxidation (133 mV dec^{-1}) and reduction (350 mV dec^{-1}), compared to the NC/I_2's Tafel slope (208 and 402 mV dec^{-1}). These results demonstrated that CoP@NC rapidly catalyzes bidirectional iodine redox processes. EIS curves in Fig. 4c showed the Nyquist plots of both electrodes between 100 kHz and 0.01 Hz before cycling. Specifically, the R_{ct} value of the CoP@NC/I_2 electrode is 29.0 Ω, fitted by the equivalent electrical circuit (Fig. 4c, inset),[17] which is smaller than that of the NC/I_2 electrode (160.0 Ω), suggesting the fastest charge-transfer kinetics in the CoP@NC/I_2 electrode. Fig. 4d summarizes the mechanism of the CoP@NC host promoting the iodine conversion process. Unlike the NC, which only physically restricts iodine species and results in slow iodine conversion, the CoP@NC host has highly exposed active sites, enhances the binding ability with intermediates, and thereby improves the catalytic iodine conversion kinetics.[21–23] Besides, the good contact interface between CoP and the carbon substrate can promote electron transfer.[7,21] This synergistic effect achieves fast iodine conversion while effectively suppressing shuttling, ultimately improving the overall battery performance.

To further evaluate the ability of CoP@NC to limit polyiodide diffusion, static adsorption experiments were performed by immersing CoP@NC and NC in zinc triiodide solutions. As shown in Fig. 5a and Fig. S7 (ESI†), after standing for 12 hours, the solution containing CoP@NC appeared much more transparent than the solution containing NC, indicating a stronger anchoring effect of CoP@NC on polyiodides. UV-visible absorption spectroscopy (Fig. 5b) further confirmed that the supernatant of the CoP@NC-impregnated solution exhibited the lowest adsorption intensity, demonstrating the superior chemical adsorption of CoP@NC for polyiodides than NC. This strong adsorption capacity was corroborated by XPS analysis of the CoP@NC after adsorption (Fig. 5c). First, the XPS survey spectrum of the CoP@NC after adsorption of I_3^- solution in Fig. S8 (ESI†) showed peaks at ~630.6 and 618.0 eV, meaning the chemical interaction between I_3^- and CoP@NC.[2] Compared with the Co spectrum of CoP@NC (Fig. 2e), all peaks of Co 2p in

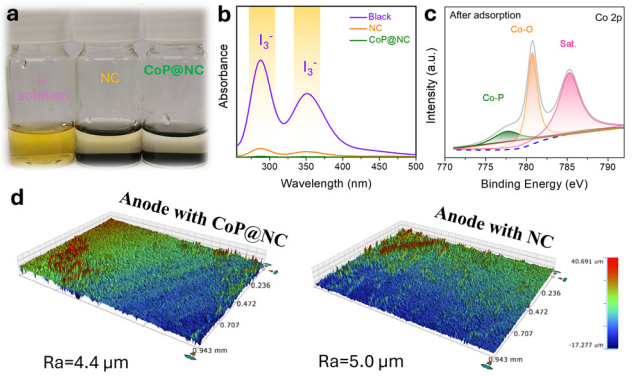

Fig. 5 (a) Visual comparison of adsorption capacity between CoP@NC and NC. (b) UV-vis spectra. (c) High-resolution XPS spectrum of Co 2p of CoP@NC–I_3. (d) 3D surface profiles of the Zn anode after cycling.

CoP@NC–I_3^- shifted in the negative direction. Specifically, the Co–O/Co–P bonds shifted from 781.6/778.5 eV to 780.7/777.5 eV, respectively, confirming the electron transfer interactions between CoP@NC and I_3^-. The above results substantiate the existence of a strong chemical interaction between CoP@NC and polyiodides rather than weak physical adsorption.[2]

To verify the role of CoP@NC in inhibiting polyiodide-related degradation, the zinc anode was carefully inspected after long-term cycling. SEM of the zinc anodes with CoP@NC and NC electrodes after 100 cycles at 1.0 A g^{-1} are shown in Fig. S9 (ESI†). The NC-based battery exhibited disordered flake/flower-like dendrites on the Zn's surface, while the CoP@NC-based battery retained an intact and smooth anode morphology. The corresponding 3D images in Fig. 5d also confirmed less byproduct coverage on the Zn's surface with the CoP@NC/I_2 cathode (4.4 μm) compared with the NC/I_2 cathode (5.0 μm), as evidenced by the reduced surface height variation. These findings certify that CoP@NC can effectively inhibit the occurrence of side reactions on the surface of the Zn anode, providing enhanced stability during cycling.

L. Z.: methodology, data curation, writing – original draft; X. G., Z. Z., Y. F., Z. Y., C. Z., and Y. W.: data curation & formal analysis. H. F., H. X., X. L. and H. L.: visualization, B. J. and H. Y.: writing – review & editing. Y. S. and T. M.: writing – review & editing, supervision, funding acquisition.

Y. S. acknowledges financial support from the National Natural Science Foundation of China (U23B20166, U21A20289, 22206011 and 21976011) and the International Joint Doctoral Education Fund of Beihang University. T. M. acknowledges Australian Research Council (ARC) through the Future Fellowship (FT210100298), Discovery Project (DP220100603), Linkage Project (LP210200504, LP220100088, LP230200897), and Industrial Transformation Research Hub (IH240100009) schemes, the Australian Government through the Cooperative Research Centres Projects (CRCPXIII000077), the Australian Renewable Energy Agency (ARENA) as part of ARENA's Transformative Research Accelerating Commercialisation Program (TM021), and European Commission's Australia-Spain Network for Innovation and Research Excellence (AuSpire). The authors also acknowledge the facilities and the technical assistance of RMIT University's Microscopy and Microanalysis Facility (RMMF) and Nano Research Facility (MNRF).

Data availability

Data are contained within the article and ESI.†

Conflicts of interest

There are no conflicts to declare.

Notes and references

1 G. Liang, B. Liang, A. Chen, J. Zhu, Q. Li, Z. Huang, X. Li, Y. Wang, X. Wang, B. Xiong, X. Jin, S. Bai, J. Fan and C. Zhi, *Nat. Commun.*, 2023, **14**, 1856.
2 L. Zhu, X. Guan, Y. Fu, Z. Zhang, Y. Li, Q. Mai, C. Zhang, Z. Yuan, Y. Wang, P. Li, H. Li, D. Su, B. Jia, H. Yu, Y. Sun and T. Ma, *Adv. Funct. Mater.*, 2024, **34**, 2409099.
3 Z. Li, W. Cao, T. Hu, Y. Hu, R. Zhang, H. Cui, F. Mo, C. Liu, C. Zhi and G. Liang, *Angew. Chem., Int. Ed.*, 2023, e202317652.
4 P.-F. Zhang, J.-H. Li, S.-J. Zhang, D.-C. Li, S.-Y. Zeng, S.-L. Xu, Q.-X. Yao, L.-Y. Liu, L. Ding, H.-X. Li, Y.-Y. Hu, J.-T. Li and Y. Zhou, *Adv. Funct. Mater.*, 2023, 2306359.
5 M. Liu, Q. Chen, X. Cao, D. Tan, J. Ma and J. Zhang, *J. Am. Chem. Soc.*, 2022, **144**, 21683–21691.
6 R. Sun, M. Qu, L. Peng, W. Yang, Z. Wang, Y. Bai and K. Sun, *Small*, 2023, **19**, 2302092.
7 L. Ji, J. Wang, X. Teng, T. J. Meyer and Z. Chen, *ACS Catal.*, 2020, **10**, 412–419.
8 Y. Li, H. Jia, U. Ali, B. Liu, L. Li, L. Zhang, H. Wang, T. Wang and C. Wang, *Chem. Eng. J.*, 2024, **483**, 149320.
9 Q. Chen, S. Chen, J. Ma, S. Ding and J. Zhang, *Nano Energy*, 2023, **117**, 108897.
10 F.-F. Li, J.-F. Gao, Z.-H. He and L.-B. Kong, *ACS Appl. Energy Mater.*, 2020, **3**, 5448–5461.
11 L. Chai, Z. Hu, X. Wang, Y. Xu, L. Zhang, T.-T. Li, Y. Hu, J. Qian and S. Huang, *Adv. Sci.*, 2020, **7**, 1903195.
12 L. Zhu, Z. Zhang, J. Luo, H. Zhang, Y. Qu and Z. Yang, *Carbon*, 2021, **174**, 317–324.
13 L. Zhu, Y. Wang, M. Wang, M. Huang, Y. Huang, Z. Zhang, J. Yu, Y. Qu, C. Li and Z. Yang, *Carbon*, 2022, **187**, 302–309.
14 D. Yu, A. Kumar, T. A. Nguyen, M. T. Nazir and G. Yasin, *ACS Sustainable Chem. Eng.*, 2020, **8**, 13769–13776.
15 L. Zhu, Y. Wang, M. Wang, Y. Xiong, Z. Zhang, J. Yu, Y. Qu, J. Cai and Z. Yang, *Carbon*, 2021, **184**, 706–713.
16 Y. Wang, L. Zhu, J. Wang, Z. Zhang, J. Yu and Z. Yang, *Chem. Eng. J.*, 2022, **433**, 133792.
17 Y. Xiong, K. Wu, S. Hong, L. Jin, Z. Zhang, L. Zhu, M. Huang, Z. Yang and J. Cai, *J. Mater. Sci.: Mater. Electron.*, 2022, **33**, 14121–14133.
18 Y. Pan, K. Sun, S. Liu, X. Cao, K. Wu, W.-C. Cheong, Z. Chen, Y. Wang, Y. Li, Y. Liu, D. Wang, Q. Peng, C. Chen and Y. Li, *J. Am. Chem. Soc.*, 2018, **140**, 2610–2618.
19 M. Zhang, T. Zhou, G. Huang, F. Han, H. Shao, T. Hu and C. Wang, *Surf. Interact.*, 2024, **47**, 104224.
20 S. Hong, Q. Li, J. Li, L. Jin, L. Zhu, X. Meng, Y. Che, Z. Yang, Z. Zhang, J. Yu and J. Cai, *ACS Appl. Mater. Interfaces*, 2024, **16**, 35063–35073.
21 D. Du, L. Wang, R. Zheng, M. Li, Z. Ran, L. Ren, M. He, Y. Yan and C. Shu, *J. Colloid Interface Sci.*, 2021, **601**, 114–123.
22 P. Hei, C. Shu, Z. Hou, R. Zheng, T. Yang, M. Li, Z. Ran, Y. Wang, D. Mei and J. Long, *J. Alloys Compd.*, 2020, **820**, 153086.
23 L.-M. Cao, Y.-W. Hu, S.-F. Tang, A. Iljin, J.-W. Wang, Z.-M. Zhang and T.-B. Lu, *Adv. Sci.*, 2018, **5**, 1800949.